DOI: 10.1002/aenm.201703058

Article type: Progress Report

Miscibility-Function Relations in Organic Solar Cells: Significance of Optimal Miscibility in Relation to Percolation

Long Ye, Brian A. Collins[†], Xuechen Jiao, Jingbo Zhao, He Yan, and Harald Ade*

Dr. L. Ye, Dr. B. A. Collins, Dr. X. C. Jiao, Prof. H. Ade

Department of Physics, Organic and Carbon Electronics Lab (ORaCEL), North Carolina State University, Raleigh, NC 27695, United States

E-mail: hwade@ncsu.edu

Dr. J. B. Zhao, Prof. H. Yan

Department of Chemistry and Hong Kong Branch of Chinese National Engineering Research Center for Tissue Restoration & Reconstruction, Hong Kong University of Science and Technology (HKUST), Clear Water Bay, Kowloon, Hong Kong

[†]Current Address: Department of Physics and Astronomy, Washington State University, Pullman, Washington 99164, USA.

ABSTRACT

Polymer solar cells (PSCs) continue to be a promising low-cost and lead-free photovoltaic technology. Of critical importance to PSCs is understanding and manipulating the composition of the amorphous mixed phase, which is governed by the thermodynamic molecular interactions of the polymer donor and acceptor molecules and the kinetics of the casting process. In this progress report, we will clarify and define nomenclature relating to miscibility and its relevance and implications to PSC devices in light of new developments. Utilizing a scanning transmission X-ray microscopy (STXM) method, the temperature dependences of "molecular miscibility" in the presence of PCBM crystals, now referred to liquidus miscibility, are presented for a number of representative blends. An emphasis is placed on relating the amorphous miscibility of high-efficiency PSC blends at a given processing temperature with their actual device performance and stability. It is shown and argued that a system with an amorphous miscibility close to percolation exhibits the most stable morphology. Furthermore, the authorsoutline an approach to convert liquidus miscibility to an effective Flory-Huggins interaction parameter χ. Crucially, determination of

temperature-dependent amorphous miscibility paves a way to rationally optimizing the stability and mixing behaviors of PSCs at actual processing and operating temperatures.

Keywords: miscibility, percolation threshold, polymer solar cells, , , scanning transmission X-ray microscopy

1. Introduction

Polymer solar cells (PSC) based on bulk-heterojunction (BHJ) blends of conjugated polymers and organic molecules continue to be a promising renewable energy technology that possesses the advantages of being light-weight and lead-free, having mechanical flexibility and tunable color, and ability to be processed into large-area devices by using eco-friendly solvents[1-4]. From the point of view of morphology/device optimization[1, 5-10], numerous factors including molecular structures of donor and acceptor materials, donor:acceptor ratio, molecular weight, and processing parameters (annealing/coating temperature, choices of co-solvent or solvent additive, solvent annealing, etc.) come into play in determining the final morphology of a PSC and thus key performance parameters, such as open-circuit voltage (V_{oc}), short-circuit current density (J_{sc}), and fill factor (FF). For a new photovoltaic polymer or a new donor:acceptor combination, new solvents and other processing conditions are usually empirically explored and optimized within a limited range of variables. Furthermore, there is currently no widely recognized conceptual framework that allows determining the best-matched acceptor material for a given donor polymer and only by carefully considering the influences of each parameter individually can these factors be exploited. All of these variables make it extremely challenging to predict the optimal BHJ morphology and performance of PSCs when designing and using new materials[2, 7, 8, 11-14].

In the BHJ of a PSC device, the polymeric electron donor (D) and organic electron acceptor (A) materials form a complex structure and morphology with the goal of optimizing simultaneously photon absorption, exciton separation, and charge transport. Generally, the disorder and semi-crystalline (sometimes nearly amorphous) qualities of the organic/polymeric photovoltaic materials make their blends difficult to form a simple two-phase morphology with pure aggregated donor and acceptor phases.[15] A three-phase morphology (see Figure 1a) including pure donor aggregates, pure acceptor aggregates, and amorphous intermixed portions (consisting of dispersed fullerene in the mostly amorphous polymer) have been previously observed or inferred by us and others in a wide range of PSC material systems[16-20]. Recent Kinetic Monte Carlo simulations[21] have suggested that this three-phase morphology may be favorable as the electronic structure of both the donor and acceptor depends on the level of aggregation, thus providing an electronic landscape that can help to sweep out charges created in the mixed phases. Molecular dynamics simulations of a matrix of polymer:acene blends pointed to the significance of thermodynamic molecular interactions in determining the formation of BHJ morphologies[14]. Practically, these molecular interactions determine an upper limit of purity of the mixed phases in the blend films[22], which will likely impact charge creation and recombination processes in devices[13, 17, 23, 24].

Experimental studies suggest that “miscibility” plays a key role in explaining the device performance of donor:fullerene systems. However, the term “miscibility” and “mixing” is used without precision and describes often different concepts. We will propose a nomenclature that should provide more clarity and for ease of reference provide a glossary below. Although at times the concept of miscibility is used to describe some average property of the morphology, we will refer to miscibility only in the context of defined thermodynamic states that relate to the binodal and

liquidus boundaries in phase diagrams, which define equilibria in amorphous-amorphous or crystalline-amorphous systems, respectively.

The relevance of miscibility to PSC device has been studied the most in polythiophene:fullerene systems. For instance, so-called "molecular miscibility" was observed in a benchmark system P3HT:$PC_{61}BM$ in two pioneering demixing experiments[16, 17] by the Ade group, and in bilayer interdiffusion work performed by the Chabinyc[19] and Russell[25] groups. Treat *et al.*[26] later linked the polymer-fullerene miscibility to charge collection efficiency and power conversion efficiency, with similar relations observed, amongst others, by Collins *et al.*[27] and Ma *et al.*[28]. The work by Vakhshouri *et al.*[29] suggested the electron transport within the BHJs depends strongly on the composition of the mixed domains. We note that the prior literature was somewhat confusing on the subject and used the term "molecular miscibility" and/or simply "miscibility" for different things, i.e., the composition of the mixed domains no matter how far from equilibrium, as well as the composition of the mixed domains in local thermodynamic equilibrium in the presence or absence of PCBM crystals. We make clear distinctions here. If a mixed domain is quenched, we will simply refer to its composition. If that composition is in local thermodynamic equilibrium in the absence of PCBM crystals, we refer to it as amorphous miscibility and in the presence of PCBM crystals as liquidus miscibility. The latter takes into account that the chemical potential of the PCBM crystals lowers the PCBM concentration of the mixed domains at equilibrium. The liquidus PCBM miscibility is thus always lower than the amorphous PCBM miscibility, a distinction first discussed and beautifully explored by interdiffusion experiments by DeLongchamp *et al.* and Richter *et al.*[30, 31]. The earlier reference by Watts *et al.*[16] to the binodal for the determination of the PCBM concentration near a PCBM crystal is incorrect, as not the amorphous miscibility but the liquidus miscibility was measured.

Much of the literature made no explicit mention if the amorphous or liquidus miscibility is measured and discussed.

Although the presence of mixed phases in bulk heterojunction PSC devices is emerging as a consensus and the phases even in the most efficient polymer:fullerene systems[32] are not pure, the amorphous miscibility of a large class of low band gap and often high-efficiency polymers and fullerene blends have not been well understood to date, in part because of the complications arising from the chemical potential of PCBM crystals. Since the amorphous miscibility is critical for many of the device parameters and PCBM crystallization is suppressed in actual devices, measuring thermodynamic interaction and the amorphous miscibility might thus be used to predict device morphology and performance.

To achieve a rational guidance for performance optimization, the amorphous miscibility or degree of molecular mixing in the mixed phases needs to be quantitatively determined and well understood at the actual processing temperatures. To achieve this goal and span the arc of concepts needed, we present and discuss the following concepts. First, we present the determination and application of liquidus miscibility and its temperature dependence of polymer solar cells by synchrotron radiation-based scanning transmission X-ray microscopy (STXM, schematically depicted in Figure 1c). We provide an overview of the liquidus miscibility method as quantified by STXM for a broad range of PSC materials systems. The temperature dependence of the liquidus miscibility is presented for representative PSC blends including previously unpublished results. Next, we focus specifically on how said liquidus miscibility relates to morphology and device operation of many high-performance polymer:fullerene systems including the former record-breaking PffBT4T-C_9C_{13}:$PC_{71}BM$ system at actual processing/working temperatures[33]. Finally, we outline an approach

to convert the STXM derived miscibility and its temperature dependence to an effective Flory-Huggins interaction parameter χ for a given temperature using χ-φ phase diagrams (Figure 1b) and complementary methods (differential scanning calorimetry, etc). This approach is expected to be a unique methodology for investigating the thermodynamics of PSCs and related electronics that use polymer mixtures.

2. Quantification of Miscibility via STXM

Experimental determination of "molecular miscibility" is an important discovery in the field of PSC[16, 17]. Although amorphous and/or liquidus miscibility can also be determined by secondary ion mass spectrometry (SIMS)[26], transmission electron microscopy[35], spectroscopic ellipsometry[30, 31], and neutron reflectivity/scattering[36], here we mainly focus on the liquidus miscibility quantified by STXM[34] as it has been used the most to make miscibility measurements. Due to the distinct molecular resonances of polymer and fullerene at energies near the carbon 1s absorption edge, STXM can provide quantitative information about the residual weight fraction of fullerene in a polymer matrix[17]. Using this methodology, Watts *et al*. discovered limited purity in the mixed domains, i.e. miscibility, but paid little credence to its implications[16]. Only Collins *et al.*[17] later successfully demonstrated and discussed the three-phase morphology of P3HT:$PC_{61}BM$ system in the context of miscibility and the limits it imposes on the purity of the mixed domains. To further probe this possibility and its implications beyond the benchmark P3HT:PCBM system, the "miscibility" of common fullerenes in a number of new low bandgap polymers[22, 27, 28, 32, 37-40] has been measured directly via STXM on films brought to thermodynamic quasi-equilibrium. We note that the residual

PCBM weight fraction in these publications was often referred to as “miscibility” as a short hand. It is imprecise as it did not correct for the volume fraction of the polymer that was crystalline. While the use of the raw STXM residual PCBM concentrations labeled “miscibility” was sufficient to make qualitative comparisons between systems and qualitative arguments about performance, we seek here to introduce the more precise use of terminology in an effort to develop more quantitative structure-function-performance relations that are rooted in thermodynamics. We will consequently refer to raw STXM measurements without correcting the degree of crystallinity as uncorrected liquidus miscibility. Particularly, uncorrected liquidus miscibility has been reported for a broad range of high-efficiency polymer:fullerene photovoltaic blends (see **Figure 2**). An amorphous mixed phase is always observed, along with a fullerene-rich phase and possibly a pure polymer phase depending on the degree of crystallinity (DoC) of the polymer. All results summarized in **Table 1** show a non-zero miscibility of PCBM in photovoltaic polymers, suggesting that all PSC devices using these material systems produce an amorphous mixed phase that consists of polymer and PCBM.

Here, we describe and illustrate the procedures of a STXM miscibility test by taking a regioregular P3HT (regioregularity=98%):$PC_{61}BM$[17] system as an example. After aggressive annealing at 180 ^{o}C for three days, the blend film of P3HT:$PC_{61}BM$ reach (local) thermal equilibrium and exhibit fullerene crystals embedded in a uniform matrix that is without depletion gradients, as evidenced by the representative STXM image shown in **Figure 3**a. Figure 3b represents the fit of the NEXAFS spectra from the depleted matrix region between the crystals for P3HT:$PC_{61}BM$ blend film annealed at 180 ^{o}C. The residual fullerene concentrations were determined by fitting the spectrum of the matrix to reference spectra of the polymer and PCBM. As shown in Figure 3b, the residual fullerene

weight fraction (uncorrected miscibility value of fullerene in the total polymer) within the depleted regions is 10.7% as determined by a linear combination of the neat reference spectrum of polymer and fullerene following previously published methods[41]. We can further convert this measured fullerene weight ratio (*w*) to fullerene volume fraction (*v*) in the polymer matrix using

$$v = \frac{w}{(1-w)\frac{\rho_{polymer}}{\rho_{PCBM}}+w} \quad \textbf{(Equation 1),}$$

where $\rho_{polymer}$ is the average density of polymer donors and ρ_{PCBM} the density of the amorphous fullerene in the mixed domains. Here we assume their densities according to literature reports[42] (e.g., 1.15 g/cm^3 for polymer donors and 1.3 g/cm^3 for amorphous PCBM).

To convert the fullerene volume fraction (*v*) in the overall polymer matrix to the polymer composition (φ) in an amorphous mixed phase, the crystalline portions of the donor polymers must be excluded. Then, we can get the polymer composition based on

$$\phi = 1 - \frac{v}{1-DoC} \quad (\textbf{Equation 2}),$$

where DoC is the degree of crystallinity of the donor polymer, which represents the volume fraction of the crystalline portion of a polymer. Quantitative analysis of DoC[43-45] is complex and has been established for some semi-crystalline polymers utilizing a number of methods. Using the STXM-measured fullerene weight fractions as well as determined or estimated DoC, one can get the polymer composition that is relevant to the coexistence curve (binodal) in a χ-φ phase diagram (Figure 1b) after the chemical potential of fullerene crystals has been accounted for. We will outline the full procedures below.

3. Temperature Dependence of Miscibility

The liquidus miscibility of polymer:fullerene systems is temperature dependent. As mentioned above, the uncorrected liquidus miscibility data reported in the literature are often determined for only a certain temperature. Therefore, the temperature dependence of liquidus miscibility is largely unknown for PSC blends except for the P3HT:$PC_{61}BM$ blend[17, 48]. In 2010, Collins *et al.* reported temperature-dependent uncorrected liquidus miscibility data for three P3HT grades of varying regioregularity (see **Figure 4**a). The lowest regioregularity batch shows a two times higher miscibility compared to those of the higher regioregularity batches at the same temperature. This is in good agreement with large batch to batch variations observed in the field. It is also shown that liquidus miscibility (for negligible temperature dependent crystallinity) of all grades is increasing with temperature, which suggests an upper critical solution temperature (UCST) behavior.

Inspired by the previous works on P3HT:$PC_{61}BM$, here we subsequently measured the temperature-dependent residual PCBM concentration in several high-performance polymer donors using the same procedures. Blends of five benchmark donor polymers including a benzodithiophene-containing poly(benzodithiophene-co-thienothiophene) (PTB7)[22, 49], a poly(2,7-carbazole) derivative PCDTBT[50], a thienopyrrole-based polymer PBDTTPD[39, 51], poly(diketopyrrolopyrrole-alt-terthiophene) (PDPP3T)[52, 53], a fluorinated benzothiadiazole-based polymer PffBT4T-C_9C_{13}[33], and two kinds of fullerenes ($PC_{61}BM$ and $PC_{71}BM$), were investigated. These polymers are representative of a broad range of donor polymers increasingly used in polymer/fullerene solar cells at present and their temperature-dependent uncorrected liquidus miscibility (residual fullerene weight fraction) are

shown in Figure 4b. For each polymer:fullerene blend, data were acquired for at least three temperatures.

The temperature-dependent STXM data reveals several compelling observations. It is interesting to find that semi-conducting blends can have very different thermodynamic behavior, with 3 out of 9 systems showing lower critical solution temperature (LCST) behavior. In addition, the phase behaviors of $PC_{61}BM$ and $PC_{71}BM$ with the same donor polymer are quite different. For instance, PDPP3T:$PC_{61}BM$ and PDPP3T:$PC_{71}BM$ show the opposite temperature dependence. To be less miscible, the choice of C_{60}-based fullerene over C_{70} is advantageous for blends with PTB7. Therefore, pairing an identical donor polymer with different fullerenes may yield distinct thermodynamics. Conversely, PBDTTPD:$PC_{61}BM$ shows a lower critical solution temperature (LCST) behavior and PffBT4T-C_9C_{13}:$PC_{71}BM$ system has a typical UCST behavior. As a result, starkly different temperature dependence with upper and lower critical solutions temperatures and fullerene-dependence is found as a function of donor polymer. Likely, these differences imply that processing strategies, performance and stability can be quite different.

4. Relating Miscibility to Device Function

In this section, we are going to delineate how liquidus miscibility impacts the device morphology and performance as well as stability in some representative high-performance polymer:fullerene solar cells. It is generally recognized that miscibility determines the physical interfacial area of a donor:acceptor BHJ, which can affect the degree of non-geminate recombination and therefore the V_{oc}[23, 54]. For instance, Vandewal *et al* showed that V_{oc} varies

inversely with the interface area in a donor:fullerene system[55] while the energy of the interfacial charge-transfer state remains constant. Therefore, a reduction of miscibility will result in a lower interfacial area and likely higher device V_{oc}. Herein, we focus on the impact of miscibility to device FF and J_{sc}, rather than V_{oc}. As summarized in **Table 1**, it is interesting to note that PffBT-2OD:ICMA has the lowest liquidus miscibility of 3.2% and highest fill factor (FF) of 77% among the systems investigated. Also, two high FF (>65%) systems such as PDPP3T:$PC_{71}BM$ and FTAZ:$PC_{61}BM$ show a relatively lower liquidus miscibility of 3.5%-5%, while low-performance PBDT-DTBT shows a much higher liquidus miscibility. In the quest to improve the performance of PSCs, understanding the impacts of liquidus miscibility is therefore needed. Using several case studies, we are able to map out the complete miscibility-function relations, and a general diagram is proposed.

4.1 High Miscibility Increases Charge Recombination and Decreases Device FFs

High amorphous miscibility generally induces the development of less pure domains and often increased charge recombination. An illustrative example is a comparative study of three structurally similar (PBnDT-DTBT) polymer in polymer:fullerene solar cell devices, where the number of fluorine (F) substitutions on the DTBT unit was varied from 0 to 2 (see **Figure 5**a). As shown in Figure 5b, the bimolecular recombination of free charge-carriers was gradually reduced as the number of fluorine increased. Stuart *et al.*[37] suggested that higher device FF and average domain purity quantified by resonant soft X-ray scattering are correlated with an observed decrease in fullerene liquidus miscibility in the polymer, which drops from ~21% (PBnDT-DTBT) to ~12% (PBnDT-DTffBT). The higher purity, caused by the observed lower miscibility with PCBM as F number is increased, likely

reduces bimolecular recombination, leading to improved device FF and PCE. This change in miscibility contributes to the device PCE increasing from ~4% in the case of the nonfluorinated polymer to over 7% for the doubly fluorinated polymer. In this case study, the uncorrected liquidus miscibility from STXM measurements is clearly anticorrelated with the bimolecular recombination and device FF. As fluorination is one of the most popular methods to optimize the photovoltaic polymers and improve device performance in the field[56], the "fluorine" impact shown in the PBnDT-DTBT case suggest reduced liquidus and by implication amorphous miscibility may be a possible reason for the enhanced performance via a fluorine substitution approach.

4.2 Loss of Fullerene Percolation Decreases the Charge Transport and Device J_{sc}

Although an anti-monotonic trend of liquidus miscibility and device performance metrics is observed in many cases, a reduction of device performance may occur when the amorphous miscibility is too low. Considerable research efforts were placed on the PBDTTPD:$PC_{61}BM$, which is a high-efficiency BHJ system that is able to provide a high V_{oc} close to 1 V and 7-8% PCE[39, 51, 57]. It was found that device PCE and EQE of PBDTTPD:$PC_{61}BM$ BHJs decrease dramatically with thermal annealing temperature (**Figure 6**a and 6b) and the BHJs lose PCE even the annealing temperature is as low as 50 °C. Bartelt *et al*.[39] demonstrated the impact of the concentration of $PC_{61}BM$ in the mixed phases on device performance of the PBDTTPD:$PC_{61}BM$ BHJ mixture by varying the annealing temperature. First, the as-cast weight ratio of $PC_{61}BM$ mixed in PBDTTPD was determined to be at least 25±5% using grazing incidence X-ray diffraction (Figure 6c), which is above the percolation threshold (~20 wt%) suggested by Vakhshouri and co-workers[29]. The measured $PC_{61}BM$ weight ratio

obtained from STXM (Figure 6d) is ~20%, ~11%, and ~6% for the 150 ^{o}C, 180 ^{o}C and 200 ^{o}C thermally annealed BHJs, respectively. These temperature-dependent liquidus miscibility results indicate that thermal annealing drives $PC_{61}BM$ to diffuse out of the mixed phases of PBDTTPD:$PC_{61}BM$ BHJs at elevated temperature and significantly decreases the concentration of $PC_{61}BM$ mixed in the amorphous PBDTTPD below the percolation threshold needed for efficient electron transport. As such, the decreased miscibility of polymer and fullerene in the amorphous phases decreases the probability of exciton dissociation and leads to increased monomolecular recombination to due to the formation of PCBM islands. It is thus necessary to have sufficient percolation pathways of all charge carriers including electrons traveling via PCBM molecules out of the device.

4.3 Too Low Miscibility Induces Burn-in Degradation of PffBT4T Polymers

Beyond an influence on device operation, the intrinsic amorphous miscibility determines the morphology stability if the morphology has to be quenched inside the binodal (Figure 1b) for best performance. Of particular relevance to this subject are low bandgap poly(difluorobenzothiadiazole-alt-quaterthiophene) (PffBT4T) polymers (see **Figure 7**a)[32, 58-61] such as PffBT4T-2OD (also known as PCE11) and its derivatives. These PffBT4T polymers stand for the best options for top performing polymer:fullerene devices and a class of high performance conjugated polymers with excellent power conversion efficiency over 10% in many fullerene and non-fullerene systems. Optimization the alkyl chains of PCE11 created a new polymer PffBT4T-C_9C_{13}[33], which can be processed with hydrocarbon solvents and afford a certified efficiency of 11.5%. It was shown that controlling the temperature dependent aggregation by preheating the substrates is the key to achieve such high

performance. Annealing sequences on two PffBT4T-2OD:fullerene blends monitored by resonant soft X-ray scattering revealed that the non-annealed devices exhibited a root-mean-square composition variation of ~90% of the asymptotic amorphous miscibility limit[32] (Figure 7b and 7c), which corresponds to an unusually low residual concentration or uncorrected liquidus miscibility of 3.2% fullerene in the polymer matrix as measured by STXM. We note the $PC_{71}BM$ concentration of the PffBT4T-OD:$PC_{71}BM$ mixed domains is larger at optimal processing conditions than the asymptotic limit. As a consequence, this inherently low miscibility will result in a significant loss of electron percolation pathways and thus affect device J_{sc} eventually as the domains purify even at room temperature towards the binodal limit. Recent studies by Brabec *et al.*[62, 63] suggested that indeed the nanomorphology of PffBT4T-2OD:$PC_{61}BM$ is kinetically trapped and the phase separation occurs spontaneously even when stored in a dark inert atmosphere environment for five days (Figure 7d). Interestingly, the PffBT4T-2OD:$PC_{61}BM$ devices stored at low temperature (220 K) show much lower degradation on J_{sc} compared with devices at room temperatures (see Figure 7e), strongly suggesting a diffusion process as a cause.

These studies motivate us to further understand the thermodynamics of PffBT4T-based systems. Accordingly, a structurally similar yet higher-efficiency PffBT4T-C_9C_{13}:$PC_{71}BM$ was used to test our hypothesis. We found this system also show very low STXM "miscibility" (<10%) at processing/working temperature. As shown in Figure 7f, we observed an over 10% decrease in J_{sc} after aging a freshly fabricated device in dark for five days while the open-circuit voltage (V_{oc}) and device fill factor (FF) remains similar. It should be stressed that this burn-in loss is quite consistent with Brabec's studies and clearly suggests this high-efficiency PffBT4T-C_9C_{13}:$PC_{71}BM$ is not stable due to the spontaneous phase demixing and the ability of PCBM to diffuse at room temperature. The low

miscibility implies the polymer purity of amorphous mixed domain in the thermodynamic limit is too high (φ>0.9) according to the χ-φ phase diagram as shown in Figure 1b, also leading to a poor J_{sc} and PCE after aging. To achieve a desirable performance in the short term, this kind of system must be quenched to an optimal phase purity using the temperature dependent aggregation strategy. Unfortunately, if this morphology is not sufficiently kinetically stabilized via vitrification and low PCBM diffusion coefficients, the device performance will degrade eventually. The amorphous miscibility can determine the stability of device active layers, which may vary widely between materials systems. Amorphous miscibility at actual processing and operating temperatures should be generally considered for the optimization of morphology stability and lead to the composition of the mixed domains close to the percolation threshold.

4.4. A Thermodynamic Diagram for Complete Miscibility-Function Relation

Studying the above-mentioned representative systems with STXM miscibility experiments enabled us to infer the complete miscibility-function relations. If a polymer:fullerene blend is highly miscible, the mixed phases will have fullerene concentration much beyond the fullerene composition for electron percolation and the volume fraction of amorphous mixed phases is large, so the recombination will be enhanced. Conversely, if the blend is too immiscible, the charges will be trapped in the pure donor or acceptor aggregates if there is a lack of sufficient percolation pathways in the amorphous mixed phases. In this low miscibility case, the phase evolution of the blend during film formation needs to be quenched for best performance, are thus unstable and eventually produce fullerene islands during aging that trap charges. We argue that the amorphous mixed phase

has a small volume fraction and a fullerene concentration near the percolation threshold in the ideal morphology. The reported fullerene composition threshold for electron percolation varies slightly with the system from 0.1 to 0.2 may come down to the predominant way molecules are arranged in the mixed phase[64]. For instance, φ=0.8 for RR-P3HT:PCBM[29] and φ=0.9 for PTB7:$PC_{71}BM$[65] when the fullerene percolation threshold is reached.

To illustrate a complete miscibility-function relation, we delineate here the critical role of miscibility in terms of the Flory-Huggins interaction parameter (χ) in determining device performance and stability of polymer:fullerene PSCs (see **Figure 8**). From the perspective of thermodynamics, morphological properties of polymer blends and polymer solutions depend critically on the Flory-Huggins interaction parameter (χ), which is a measure of the net enthalpic interaction energy (in units of kT and per unit volume) upon exchange of constituent units from a like (demixed) to an unlike (mixed) environment. The larger this net exchange energy, the larger χ. In balance with the entropic gain of exchange, χ controls the degree of molecular mixing between the components. The binodal composition along the coexistence curve of the χ-φ phase diagram determines the maximum achievable purity in the amorphous mixed phase when the PCBM crystallization is suppressed kinetically during the device fabrication. For a given polymer:fullerene system, best device FF and PCE can be obtained when only optimum amorphous miscibility and thus optimal χ with a binary composition near the percolation threshold[29, 65]. A system with an amorphous miscibility close to this optimum value during normal device operating conditions exhibits most likely stable morphology (short of PCBM crystallization) and thus intrinsically meta-stable operation. The coexistence curve in cases where the small molecule can crystallize is therefore referred to as meta-stable miscibility gap. PffBT4T-C_9C_{13}:$PC_{71}BM$ has an amorphous miscibility that is too low (below the fullerene percolation

threshold) at processing and/or operating conditions and this system needs to be quenched into a morphology for highest efficiency that has not yet reached the metastable state determined by its binodal[62]. Crucially, the temperature dependent miscibility can also explain additional observations in the literature. PCDTBT:$PC_{71}BM$ is one of the most stable polymer:fullerene systems reported in the literature[66, 67]. For instance, it is thermally stable in air at annealing temperature up to 150 °C[66] and demonstrates so far the longest operation lifetime of nearly 7 years[67]. This high stability can be well understood by our miscibility-function relation as its amorphous miscibility[68] at actual processing temperature is very close to the fullerene percolation threshold. These observations together suggest that BHJ systems with an optimum miscibility should be used to limit fullerene diffusion and improve the morphological stability of PSCs.

The length-scale of PSC device morphologies is likely kinetically quenched in, as observed by real-time studies[69-74], during the early stages of casting as the polymer crashes out of solution. The level of mixing in the amorphous polymer-rich mixed domains is likely determined by Flory-Huggins χ as the film dries and evolves towards (local) thermodynamic equilibrium represented by the binodal composition. Consequently, determining miscibility or χ at processing temperature can serve as a feasible tool to predict device performance and in turn guide the choice of processing conditions where the binodal composition is close to the fullerene percolation threshold. Determining miscibility at the operating condition will likely predict the device stability.

5. Converting temperature dependent miscibility to χ(T)

In this section, we will overview the determination of the Flory-Huggins interaction parameter χ and introduce a unique methodology (including theoretical background, general procedures, and a specific example) to extract Flory-Huggins χ(T) from temperature dependent STXM miscibility data.

5.1 An Overview of χ Determinations

It is generally acknowledged that both simulation and determination of Flory-Huggins interaction parameter (χ) are challenging tasks for polymeric blends[31, 75-79]. To date, cloud-point measurement[80], solubility parameters[81], scattering[82] and differential scanning calorimetry (DSC)[83] methods have been used for χ determination, but the measurements often cover only a limited temperature range or are confounded by the presence of crystalline fractions of the materials. For instance, DSC can only measure χ at/near the melting temperature [84, 85], which is far above the temperatures used in actual processing. Solubility parameters only provide χ at room temperature and are not accurate[31]. Also, the positive χ values derived from solubility parameters completely fail to explain miscible polymer blends, in which negative χ is observed from DSC measurements[86]. Although a few groups have determined the χ parameter of the well-known poly(3-hexylthiophene) (P3HT) and fullerene at the melting temperature using DSC melting point depression[35, 84, 85] or calculated χ for some high performance systems at room temperature using the semi-empirical or empirical solubility parameters[5, 12, 63, 87-90], the temperature dependence of χ, i.e., χ(T) is still not available so far for most PSC blends. Reliable measurement of Flory-Huggins χ(T) is therefore of great value for the fundamental understanding and practical applications in polymer electronics and towards quantitative structure-function relations.

5.2 Theory of χ(T) Methodology

Quantification of temperature-dependent STXM miscibility offers a new conceptual approach to determine the Flory-Huggins χ(T). We follow the tradition widely used in the community[81, 91], where non-ideal behavior away from classical, as conceived Flory-Huggins mean field theory is packed into the temperature dependence of χ, so that both UCST and LCST systems are mapped onto a single χ-φ diagram. Since the binodal curve can be simulated for a certain polymer:small molecule blend with known molecular weights of components, the effective χ can be extracted at a certain temperature by inputting the coexistence composition to the simulated χ-φ phase diagram (Figure 8). Generally, χ is a function of reciprocal absolute temperature (T)[78, 82], i.e., $\chi=A+B/T$, where A and B are temperature independent constants (assuming the DoC is not that different for the temperature range investigated), and T is the absolute temperature (K). Once A and B constants are determined, one can predict χ at any processing or working temperatures. Potentially, a χ with a more complex phenomenological temperature dependence ($\chi=A+B/T+C/T^2$) is possible[92, 93]. Using at least three (T, φ, χ) points, one can extract the effective χ(T) by fitting to phenomenological temperature dependence and extrapolate it to the actual process temperature.

According to the self-consistent treatment of crystalline-amorphous polymeric systems[94, 95], the total free energy of mixing for an amorphous polymer and PCBM blend system can be described by

$$f(\psi,\phi) = \phi f(\psi) + \frac{\phi}{N}\ln(\phi) + (1-\phi)\ln(1-\phi) + \chi_{\text{effective}}\phi(1-\phi) \qquad \textbf{(Equation 3)},$$

where effective χ covers all possible interactions involving amorphous-amorphous and crystal-amorphous interactions, as shown in **Equation 4**.

$$\chi_{\text{effective}} = \chi_{aa} + \chi_{ca}\psi^2 \qquad \textbf{(Equation 4)}$$

where $f(\psi)$ is the variation of free energy of crystallization. χ_{aa} is the Flory-Huggins interaction parameter representing the amorphous-amorphous interaction. χ_{ca} represents the crystal-amorphous interaction parameter, which is proportional to the enthalpy of crystallization or melting (ΔH), i.e., $\chi_{ca} \propto \Delta H/RT$. N is the degree of polymerization (or the number of repeating unit) of a donor polymer. ψ is the crystal order parameter of PCBM and, on account of PCBM being a small molecule, is assumed to be 1 over the temperature range probed in STXM.

In our STXM miscibility measurements, the liquidus miscibility represents the thermodynamic limit of fullerene concentration in the amorphous regions of the polymer-rich domains in the presence of PCBM crystals. For crystalline-amorphous systems (see **Figure 9**), the PCBM is made to crystallize such that the system reaches the coexistence composition, i. e. the liquidus, which can be subsequently experimentally determined. Above the liquidus the system is entirely liquid, and below the liquidus, the system consists of two-phases that comprise PCBM crystals and a liquid mixture with the composition of the liquidus. Below the glass transition temperature T_g, the system is frozen into a glass and the liquidus would be the equilibrium composition between the amorphous, mixed solid and the PCBM crystals. These phase transitions are controlled by the $\chi_{aa}(T)$ and the chemical potential of the PCBM crystals. To correct for the crystal-amorphous interaction, χ_{ca} can be determined from DSC melting point depression of PCBM using

$$1 - \frac{T_m}{T_m^0} = \frac{RT_m}{\Delta H}\chi_{ca}(1-\phi) \qquad \textbf{(Equation 5)},$$

where T_m^0 is the melting point of neat PCBM. χ_{ca} at melting points can be determined by **Equation 6** from the slope, *S*, of the $(1-T_m/T_m^0)$ against $(1-\varphi)$ plot.

$$\chi_{ca}(T_m) = S\frac{\Delta H}{RT_m} \quad \textbf{(Equation 6)}$$

5.3 Conversion to χ(T): A Case Study

Here we outline the specific routes for Flory-Huggins χ(T) measurements of polymer:fullerene systems by using PCDTBT:$PC_{71}BM$ as an example. As PCDTBT is a highly amorphous polymer. There are no $PC_{71}BM$ crystals in the PCDTBT:$PC_{71}BM$ devices, hence only χ_{aa} is active and dominates the effective χ for PCDTBT:$PC_{71}BM$ devices. Thus for the conversion of the STXM miscibility data to $\chi_{aa}(T)$, we need to correct for χ_{ca}. By fitting to the melting point depression of $PC_{71}BM$ of the PCDTBT:$PC_{71}BM$ system (data not shown here), a slope *S* of 0.121 is obtained based upon Equations 5 and 6. The melting enthalpy (ΔH) of $PC_{71}BM$ is 10.2 J/g and the melting point (T_m) of neat $PC_{71}BM$ is 317.7 °C, thus $\chi_{ca}(T_m)$ is ~0.26. Hence, $\chi_{ca}(T)$ can be obtained based on the $\chi_{ca}(T) \propto 1/T$ relation. By subtracting from the effective χ(T) obtained from STXM data the $\chi_{ca}(T)$ derived from DSC data, we calculate $\chi_{aa}(T)$ as shown in **Figure 10**. Therefore, the $\chi_{aa}(T)=-1.57+1063/T$ is determined for PCDTBT:$PC_{71}BM$, taking into account the chemical potential of the dispersed PCBM crystals created. In this way, the STXM measurements are converted and can be extrapolated to achieve the $\chi_{aa}(T)$ as exemplified in **Figure 10** over a temperature range relevant for OSC devices.

5.4 Summary of χ(T)

Lastly, we summarize our unique measurements of Flory-Huggins χ(T) for OSC systems. In purely amorphous-amorphous situations, binodal measurements by SIMS[68] for example can be directly converted to Flory-Huggins χ(T) by using Flory-Huggins theory. Usually, only PCBM aggregation but no crystallization is observed for typical PSC devices as they are processed below the glass transition temperature of the PCBM. For systems in which one or both components are able to crystallize, the conversion to a Flory-Huggins χ that reflects purely the amorphous interactions (the dashed lines in **Figure 9**) is more complex and needs to be adjusted for the chemical potential of the crystals. Of critical importance is the extraction of the metastable miscibility gap[94]. Using the STXM method, we can measure the coexistence composition of the liquidus in aggressively annealed blends. These phase transitions are controlled by an effective χ, and the inversion yields a χ(T). To make it device relevant, this data needs to be adjusted for the crystallization of the PCBM, which is, to first order, a slowly varying correction[95], as the crystal-amorphous interaction parameter (χ_{ca}) is assumed to be scaling with $\chi_{ca} \sim \Delta H/RT$ and is not varying as strongly as χ_{aa}, where ΔH is the melting enthalpy of neat PCBM and T is the absolute temperature. The scaling can be calibrated to match the χ at the melting point (T_m), which can be derived from DSC melting point depression. Combining STXM and other complementary tools (DSC, light scattering, etc) could therefore be more valuable. We also stress that there is an increasing interest in the PSC field into using thermodynamics parameters, primarily derived from the use of DSC[61, 63, 68, 84, 86, 88, 96] and surface tension measurements[89, 97, 98]. Together, our STXM methodology is critical for interpolating the χ(T) between the surface tension measurements at RT and DSC measurements at T_m.

6. Outlook and Conclusion

In summary, we highlight the significance of miscibility and its temperature dependence in understanding the important aspects of morphology, performance, and stability of polymer:fullerene solar cells. Using STXM as a primary tool, highly variable temperature dependences of miscibility and phase behaviors, i.e. upper and lower critical solution temperatures, were observed for a wide range of BHJ systems. Starkly different fullerene-dependence is found as a function of polymer donor. A high miscibility results in the development of excessively impure domains, which increases bimolecular recombination, thereby decreasing device J_{sc} and FF. In contrast, a miscibility that is too low results in strong burn-in degradation of polymer:fullerene devices as exemplified in the cases of record-breaking PffBT4T derivatives. There is an optimum miscibility/Flory-Huggins χ with a binodal composition near the fullerene percolation threshold. Importantly, a system with a χ close to this optimum value during normal device operating conditions exhibits most likely stable morphology and thus operation. In addition, we introduce the more precise use of terminology in an effort to develop a more quantitative structure-function-performance relation that is rooted in thermodynamics. Notably, the quantification of temperature-dependent miscibility is also capable of determining Flory-Huggins $\chi(T)$ for both amorphous and crystalline polymer systems. The thermodynamic interactions of key constituent materials will allow us to establish their relation to (quenched and metastable) morphology in actual organic devices and their performance.

In order to predict the best processing route of a new material combination, one needs to measure miscibility and its temperature dependence. Although the miscibility presented here was measured by synchrotron radiation-based STXM, visible light/optical microscopy and UV-vis spectroscopy are readily accessible to the community and a combination of these tools could potentially be a replacement of the synchrotron-based miscibility characterizations, thus making our concepts more

widely usable. Additionally, our quantification of temperature-dependent miscibility may enable researchers to correlate miscibility/χ to charge creation[99], charge recombination[100], and exciton diffusion[101] of PSCs in actual operating temperatures. We note that hundreds of non-fullerene small molecule acceptors[102-119] are created to replace fullerene acceptors in the PSC field, and the impact of miscibility needs to be understood. Miscibility/χ-function relations have been investigated in a few of nonfullerene OSC systems [5, 68, 88, 120], all of which point to a similar trend that high χ is a prerequisite of high domain purity and thus likely high device FF. More work is required to quantify the temperature dependence of amorphous miscibility/χ of these emergent systems and how that relate to the actual performance and stability. Recent studies also revealed the importance of miscibility in understanding the working mechanisms of ternary blend PSCs[86, 121-124]. The methodology established here should be able to provide valuable guidelines for optimizing these emerging systems. We believe that tailoring of the miscibility between donor and acceptor materials is the key to high-performing, highly stable and, therefore, economically viable organic photovoltaic technologies.

Glossary

For clarity, definitions of the most important terms used in this Progress Report are listed below:

Amorphous miscibility: The composition of the mixed, amorphous domains in local thermodynamic equilibrium in the absence of PCBM crystals.

Binodal: In polymer thermodynamics, the binodal, also known as the coexistence curve in binary amorphous mixtures, denotes the condition at which two distinct phases may coexist.

Chemical potential: The change in Gibbs free energy with respect to change in amount of the component, with pressure, temperature, and amounts of other components being constant. Phases are in equilibrium if their chemical potentials are equal.

Critical point: In polymer thermodynamics, critical χ_c is the χ at the critical point, where the binodal and spinodal curves intersect. The corresponding temperature and composition of χ_c are called critical temperature and critical composition, respectively.

LCST: Lower critical solution temperature (LCST) is the critical temperature below which the components of a mixture are miscible for all compositions.

FH: FH often refers to Flory-Huggins solution theory and is a mathematical model of the thermodynamics of polymer solutions that takes account of the great dissimilarity in molecular sizes in adapting the usual expression for the entropy of mixing.

Flory-Huggins Interaction parameter: This dimensionless quantity was originally introduced by Paul J. Flory and Maurice L. Huggins as an exchange interaction parameter in their lattice model of polymer solutions[93]. For this reason, this parameter is often called Flory-Huggins Parameter or χ. χ characterizes the interaction energy per unit volume divided by kT and is directly related to the molecular energy of interaction between the two components of a binary system. In practice, χ is often used includes non-ideal FH characteristics, such as an entropic term.

Liquidus: A curve in a graph of the temperature and composition of a mixture, above which the substance is entirely liquid.

Liquidus miscibility: The composition of the mixed, amorphous domains in local thermodynamic equilibrium in the presence of PCBM crystals.

Melting Point Depression: It is the phenomenon of reduction of the melting point of a material with reduction of its purity. Nishi and Wang[83] derived a relationship describing the melting point depression of a crystalline polymer due to the presence of a miscible diluent.

Spinodal: In polymer thermodynamics, the limit of local stability with respect to small fluctuations is clearly defined by the condition that the second derivative of Gibbs free energy with respect to density or some composition variable is zero. The locus of these points is known as the spinodal curve.

UCST: Upper critical solution temperature (UCST) is the critical temperature above which the components of a mixture are miscible in all proportions.

Supporting Information

Supporting Information is available from the Wiley Online Library or from the author.

Conflict of Interest

The authors declare no conflict of interest.

Acknowledgements

L.Y., X.J., and H.A. gratefully acknowledge the support by ONR grants N00141512322 and N000141712204. Early measurements by B.C. were supported by the U.S. Department of Energy, Office of Science, Basic Energy Science, Division of Materials Science and Engineering under Contract No. DE-FG02-98ER45737. STXM miscibility data were acquired at beamline 5.3.2.2 at the Advanced

Light Source, which is supported by the Director, Office of Science, Office of Basic Energy Sciences, of the U.S. Department of Energy under Contract No. DE-AC02-05CH11231. The PffBT4T polymers by H.Y. and J.Z. were partially supported by the National Basic Research Program of China (973 Program project numbers 2013CB834701 and 2014CB643501), the Hong Kong Research Grants Council (project numbers T23–407/13 N, N_HKUST623/13, 16305915, 16322416, 606012, and 16303917), HK JEBN Limited, HKUST president's office (Project FP201) and the National Science Foundation of China (#21374090). H.Y. especially thanks Hong Kong Innovation and Technology Commission for the support through projects ITC-CNERC14SC01 and ITS/083/15. The authors appreciate the fruitful discussions with Masoud Ghasemi and acknowledge Prof. Enrique Gomez for sharing his FH code.

Received: ((will be filled in by the editorial staff))
Revised: ((will be filled in by the editorial staff))
Published online: ((will be filled in by the editorial staff))

[1] Y. Huang, E. J. Kramer, A. J. Heeger, G. C. Bazan, *Chem. Rev.* **2014**, *114*, 7006.

[2] N. E. Jackson, B. M. Savoie, T. J. Marks, L. X. Chen, M. A. Ratner, *J. Phys. Chem. Lett.* **2015**, *6*, 77.

[3] L. Ye, Y. Xiong, H. Yao, A. Gadisa, H. Zhang, S. Li, M. Ghasemi, N. Balar, A. Hunt, B. T. O'Connor, J. Hou, H. Ade, *Chem. Mater.* **2016**, *28*, 7451.

[4] S. Zhang, L. Ye, H. Zhang, J. Hou, *Mater. Today* **2016**, *19*, 533.

[5] L. Ye, W. Zhao, S. Li, S. Mukherjee, J. H. Carpenter, O. Awartani, X. Jiao, J. Hou, H. Ade, *Adv. Energy Mater.* **2017**, *7*, 1602000.

[6] S. Mukherjee, C. M. Proctor, G. C. Bazan, T. Q. Nguyen, H. Ade, *Adv. Energy Mater.* **2015**, *5*, 1500877.

[7] N. D. Treat, P. Westacott, N. Stingelin, *Annu. Rev. Mater. Res.* **2015**, *45*, 459.

[8] F. Liu, Y. Gu, J. W. Jung, W. H. Jo, T. P. Russell, *J. Polym. Sci. Part B: Polym. Phys.* **2012**, *50*, 1018.

[9] S. J. Lou, J. M. Szarko, T. Xu, L. Yu, T. J. Marks, L. X. Chen, *J. Am. Chem. Soc.* **2011**, *133*, 20661.

[10] U. Würfel, D. Neher, A. Spies, S. Albrecht, *Nat. Commun.* **2015**, *6*, 6951.

[11] N. D. Treat, M. L. Chabinyc, *Annu. Rev. Phys. Chem.* **2014**, *65*, 59.

[12] S. Kouijzer, J. J. Michels, M. van den Berg, V. S. Gevaerts, M. Turbiez, M. M. Wienk, R. A. J. Janssen, *J. Am. Chem. Soc.* **2013**, *135*, 12057.

[13] N. D. Treat, A. Varotto, C. J. Takacs, N. Batara, M. Al-Hashimi, M. J. Heeney, A. J. Heeger, F. Wudl, C. J. Hawker, M. L. Chabinyc, *J. Am. Chem. Soc.* **2012**, *134*, 15869.

[14] K. Do, C. Risko, J. E. Anthony, A. Amassian, J.-L. Brédas, *Chem. Mater.* **2015**, *27*, 7643.

[15] K. Vandewal, S. Himmelberger, A. Salleo, *Macromolecules* **2013**, *46*, 6379.

[16] B. Watts, W. J. Belcher, L. Thomsen, H. Ade, P. C. Dastoor, *Macromolecules* **2009**, *42*, 8392.

[17] B. A. Collins, E. Gann, L. Guignard, X. He, C. R. McNeill, H. Ade, *J. Phys. Chem. Lett.* **2010**, *1*, 3160.

[18] W. Yin, M. Dadmun, *ACS Nano* **2011**, *5*, 4756.

[19] N. D. Treat, M. A. Brady, G. Smith, M. F. Toney, E. J. Kramer, C. J. Hawker, M. L. Chabinyc, *Adv. Energy Mater.* **2011**, *1*, 82.

[20] D. Chen, A. Nakahara, D. Wei, D. Nordlund, T. P. Russell, *Nano Lett.* **2011**, *11*, 561.

[21] T. M. Burke, M. D. McGehee, *Adv. Mater.* **2014**, *26*, 1923.

[22] B. A. Collins, Z. Li, J. R. Tumbleston, E. Gann, C. R. McNeill, H. Ade, *Adv. Energy Mater.* **2013**, *3*, 65.

[23] S. M. Menke, N. A. Ran, G. C. Bazan, R. H. Friend, *Joule* **2017**, *2*, 1.

[24] O. Alqahtani, M. Babics, J. Gorenflot, V. Savikhin, T. Ferron, A. Balawi, A. Paulke, Z. Kan, M. Pope, A. J. Clulow, J. Wolf, P. L. Burn, G. Ian, N. Dieter, M. F. Toney, F. Laquai, P. M. Beaujuge, B. A. Collins, *Under review* **2017**.

[25] D. Chen, F. Liu, C. Wang, A. Nakahara, T. P. Russell, *Nano Lett.* **2011**, *11*, 2071.

[26] N. D. Treat, A. Varotto, C. J. Takacs, N. Batara, M. Al-Hashimi, M. J. Heeney, A. J. Heeger, F. Wudl, C. J. Hawker, M. L. Chabinyc, *J. Am. Chem. Soc.* **2012**, *134*, 15869.

[27] B. A. Collins, Z. Li, C. R. McNeill, H. Ade, *Macromolecules* **2011**, *44*, 9747.

[28] W. Ma, J. R. Tumbleston, M. Wang, E. Gann, F. Huang, H. Ade, *Adv. Energy Mater.* **2013**, *3*, 864.

[29] K. Vakhshouri, D. R. Kozub, C. Wang, A. Salleo, E. D. Gomez, *Phys. Rev. Lett.* **2012**, *108*, 026601.

[30] H. W. Ro, B. Akgun, B. T. O'Connor, M. Hammond, R. J. Kline, C. R. Snyder, S. K. Satija, A. L. Ayzner, M. F. Toney, C. L. Soles, D. M. DeLongchamp, *Macromolecules* **2012**, *45*, 6587.

[31] D. Leman, M. A. Kelly, S. Ness, S. Engmann, A. Herzing, C. Snyder, H. W. Ro, R. J. Kline, D. M. DeLongchamp, L. J. Richter, *Macromolecules* **2015**, *48*, 383.

[32] Y. Liu, J. Zhao, Z. Li, C. Mu, W. Ma, H. Hu, K. Jiang, H. Lin, H. Ade, H. Yan, *Nat. Commun.* **2014**, *5*, 5293.

[33] J. Zhao, Y. Li, G. Yang, K. Jiang, H. Lin, H. Ade, W. Ma, H. Yan, *Nat. Energy* **2016**, *1*, 15027.

[34] A. L. D. Kilcoyne, T. Tyliszczak, W. F. Steele, S. Fakra, P. Hitchcock, K. Franck, E. Anderson, B. Harteneck, E. G. Rightor, G. E. Mitchell, A. P. Hitchcock, L. Yang, T. Warwick, H. Ade, *J. Synchrotron Rad.* **2003**, *10*, 125.

[35] D. R. Kozub, K. Vakhshouri, L. M. Orme, C. Wang, A. Hexemer, E. D. Gomez, *Macromolecules* **2011**, *44*, 5722.

[36] H. Chen, J. Peet, Y.-C. Hsiao, B. Hu, M. Dadmun, *Chem. Mater.* **2014**, *26*, 3993.

[37] A. C. Stuart, J. R. Tumbleston, H. Zhou, W. Li, S. Liu, H. Ade, W. You, *J. Am. Chem. Soc.* **2013**, *135*, 1806.

[38] J. R. Tumbleston, L. Yang, W. You, H. Ade, *Polymer* **2014**, *55*, 4884.

[39] J. A. Bartelt, Z. M. Beiley, E. T. Hoke, W. R. Mateker, J. D. Douglas, B. A. Collins, J. R. Tumbleston, K. R. Graham, A. Amassian, H. Ade, J. M. J. Frechet, M. F. Toney, M. D. McGehee, *Adv. Energy Mater.* **2013**, *3*, 364.

[40] J. R. Tumbleston, A. C. Stuart, E. Gann, W. You, H. Ade, *Adv. Funct. Mater.* **2013**, *23*, 3463.

[41] B. A. Collins, H. Ade, *J. Electron. Spectrosc. Relat. Phenom.* **2012**, *185*, 119.

[42] J. W. Kiel, B. J. Kirby, C. F. Majkrzak, B. B. Maranville, M. E. Mackay, *Soft Matter* **2010**, *6*, 641.

[43] J. Rivnay, S. C. B. Mannsfeld, C. E. Miller, A. Salleo, M. F. Toney, *Chem. Rev.* **2012**, *112*, 5488.

[44] X. Shen, W. Hu, T. P. Russell, *Macromolecules* **2016**, *49*, 4501.

[45] C. R. Snyder, R. C. Nieuwendaal, D. M. DeLongchamp, C. K. Luscombe, P. Sista, S. D. Boyd, *Macromolecules* **2014**, *47*, 3942.

[46] W. Ma, J. R. Tumbleston, L. Ye, C. Wang, J. H. Hou, H. Ade, *Adv. Mater.* **2014**, *26*, 4234.

[47] W. Ma, L. Ye, S. Zhang, J. Hou, H. Ade, *J. Mater. Chem. C* **2013**, *1*, 5023.

[48] B. A. Collins, J. R. Tumbleston, H. Ade, *J. Phys. Chem. Lett.* **2011**, *2*, 3135.

[49] Y. Liang, Z. Xu, J. Xia, S.-T. Tsai, Y. Wu, G. Li, C. Ray, L. Yu, *Adv. Mater.* **2010**, *22*, E135.

[50] S. H. Park, A. Roy, S. Beaupre, S. Cho, N. Coates, J. S. Moon, D. Moses, M. Leclerc, K. Lee, A. J.

Heeger, *Nat. Photonics* **2009**, *3*, 297.

[51] C. Cabanetos, A. El Labban, J. A. Bartelt, J. D. Douglas, W. R. Mateker, J. M. J. Fréchet, M. D. McGehee, P. M. Beaujuge, *J. Am. Chem. Soc.* **2013**, *135*, 4656.

[52] L. Ye, S. Zhang, W. Ma, B. Fan, X. Guo, Y. Huang, H. Ade, J. Hou, *Adv. Mater.* **2012**, *24*, 6335.

[53] K. H. Hendriks, G. H. L. Heintges, V. S. Gevaerts, M. M. Wienk, R. A. J. Janssen, *Angew. Chem. Int. Ed.* **2013**, *52*, 8341.

[54] T. M. Burke, S. Sweetnam, K. Vandewal, M. D. McGehee, *Adv. Energy Mater.* **2015**, *5*, 1500123.

[55] K. Vandewal, J. Widmer, T. Heumueller, C. J. Brabec, M. D. McGehee, K. Leo, M. Riede, A. Salleo, *Adv. Mater.* **2014**, *26*, 3839.

[56] Q. Zhang, M. A. Kelly, N. Bauer, W. You, *Acc. Chem. Res.* **2017**, *50*, 2401.

[57] C. Piliego, T. W. Holcombe, J. D. Douglas, C. H. Woo, P. M. Beaujuge, J. M. J. Fréchet, *J. Am. Chem. Soc.* **2010**, *132*, 7595.

[58] G. Pirotte, S. Agarkar, B. Xu, J. Zhang, L. Lutsen, D. Vanderzande, H. Yan, P. Pollet, J. R. Reynolds, W. Maes, S. R. Marder, *J. Mater. Chem. A* **2017**, *5*, 18166.

[59] H. Hu, P. C. Y. Chow, G. Zhang, T. Ma, J. Liu, G. Yang, H. Yan, *Acc. Chem. Res.* **2017**, *50*, 2549.

[60] W. Ma, G. F. Yang, K. Jiang, J. H. Carpenter, Y. Wu, X. Y. Meng, T. McAfee, J. B. Zhao, C. H. Zhu, C. Wang, H. Ade, H. Yan, *Adv. Energy Mater.* **2015**, *5*, 1501400.

[61] H. Yao, Y. Li, H. Hu, P. C. Y. Chow, S. Chen, J. Zhao, Z. Li, J. H. Carpenter, J. Y. L. Lai, G. Yang, Y. Liu, H. Lin, H. Ade, H. Yan, *Adv. Energy Mater.* **2017**, *7*, 1701895.

[62] N. Li, J. D. Perea, T. Kassar, M. Richter, T. Heumueller, G. J. Matt, Y. Hou, N. S. Güldal, H. Chen, S. Chen, S. Langner, M. Berlinghof, T. Unruh, C. J. Brabec, *Nat. Commun.* **2017**, *8*, 14541.

[63] J. D. Perea, S. Langner, M. Salvador, B. Sanchez-Lengeling, N. Li, C. Zhang, G. Jarvas, J. Kontos, A. Dallos, A. Aspuru-Guzik, C. J. Brabec, *J. Phys. Chem. C* **2017**, *121*, 18153.

[64] M. B. Isichenko, *Rev. Mod. Phys.* **1992**, *64*, 961.

[65] C. H. Y. Ho, S. H. Cheung, H.-W. Li, K. L. Chiu, Y. Cheng, H. Yin, M. H. Chan, F. So, S.-W. Tsang, S. K. So, *Adv. Energy Mater.* **2017**, *7*, 1602360.

[66] S. Cho, J. H. Seo, S. H. Park, S. Beaupré, M. Leclerc, A. J. Heeger, *Adv. Mater.* **2010**, *22*, 1253.

[67] C. H. Peters, I. T. Sachs-Quintana, J. P. Kastrop, S. Beaupré, M. Leclerc, M. D. McGehee, *Adv.*

Energy Mater. **2011**, *1*, 491.

[68] L. Ye, H. Hu, M. Ghasemi, T. Wang, B. A. Collins, J.-H. Kim, K. Jiang, J. Carpenter, X. Jiao, H. Li, Z. Li, T. McAfee, J. Zhao, X. k. Chen, J. Y. L. Lai, T. Ma, J.-L. Bredas, H. Yan, H. Ade, *Nat. Mater.* **2017**, *Revised*.

[69] J. J. van Franeker, M. Turbiez, W. Li, M. M. Wienk, R. A. Janssen, *Nat. Commun.* **2015**, *6*, 6229.

[70] S. Engmann, F. A. Bokel, H. W. Ro, D. M. DeLongchamp, L. J. Richter, *Adv. Energy Mater.* **2016**, *6*, 1502011.

[71] L. Ye, Y. Xiong, S. Li, M. Ghasemi, N. Balar, J. Turner, A. Gadisa, J. Hou, B. T. O'Connor, H. Ade, *Adv. Funct. Mater.* **2017**, *27*, 1702016.

[72] L. J. Richter, D. M. DeLongchamp, A. Amassian, *Chem. Rev.* **2017**, *117*, 6332.

[73] K. W. Chou, B. Yan, R. Li, E. Q. Li, K. Zhao, D. H. Anjum, S. Alvarez, R. Gassaway, A. Biocca, S. T. Thoroddsen, A. Hexemer, A. Amassian, *Adv. Mater.* **2013**, *25*, 1923.

[74] F. Liu, S. Ferdous, E. Schaible, A. Hexemer, M. Church, X. Ding, C. Wang, T. P. Russell, *Adv. Mater.* **2015**, *27*, 886.

[75] W. Zhang, E. D. Gomez, S. T. Milner, *Phys. Rev. Lett.* **2017**, *119*, 017801.

[76] B. Kuei, E. D. Gomez, *Soft Matter* **2016**, *13*, 49.

[77] J.-M. Y. Carrillo, Z. Seibers, R. Kumar, M. A. Matheson, J. F. Ankner, M. Goswami, K. Bhaskaran-Nair, W. A. Shelton, B. G. Sumpter, S. M. Kilbey, *ACS Nano* **2016**, *10*, 7008.

[78] F. S. Bates, *Science* **1991**, *251*, 898.

[79] B. P. Lyons, N. Clarke, C. Groves, *Energy Environ. Sci.* **2012**, *5*, 7657.

[80] J. Kressler, N. Higashida, K. Shimomai, T. Inoue, T. Ougizawa, *Macromolecules* **1994**, *27*, 2448.

[81] H. B. Eitouni, N. P. Balsara, in *Physical Properties of Polymers Handbook*, (Ed: J. E. Mark), Springer New York, New York, NY 2007, 339.

[82] T. P. Russell, R. P. Hjelm, P. A. Seeger, *Macromolecules* **1990**, *23*, 890.

[83] T. Nishi, T. T. Wang, *Macromolecules* **1975**, *8*, 909.

[84] P. Westacott, N. D. Treat, J. Martin, J. H. Bannock, J. C. de Mello, M. Chabinyc, A. B. Sieval, J. J. Michels, N. Stingelin, *J. Mater. Chem. A* **2017**, *5*, 2689.

[85] F. Liu, D. Chen, C. Wang, K. Luo, W. Gu, A. L. Briseno, J. W. P. Hsu, T. P. Russell, *ACS Appl. Mater.*

Interfaces **2014**, *6*, 19876.

[86] M. Ghasemi, L. Ye, Q. Zhang, L. Yan, J. H. Kim, O. Awartani, W. You, A. Gadisa, H. Ade, *Adv. Mater.* **2017**, *29*, 1604603.

[87] N. Li, J. D. Perea, T. Kassar, M. Richter, T. Heumueller, G. J. Matt, Y. Hou, N. S. Guldal, H. Chen, S. Chen, S. Langner, M. Berlinghof, T. Unruh, C. J. Brabec, *Nat. Commun.* **2017**, *8*, 14541.

[88] H. J. Bin, Y. K. Yang, Z. G. Zhang, L. Ye, M. Ghasem, S. S. Chen, Y. D. Zhang, C. F. Zhang, C. K. Sun, L. W. Xue, C. D. Yang, H. Ade, Y. F. Li, *J. Am. Chem. Soc.* **2017**, *139*, 5085.

[89] J. H. Kim, A. Gadisa, C. Schaefer, H. F. Yao, B. R. Gautam, N. Balar, M. Ghasemi, I. Constantinou, F. So, B. T. O'Connor, K. Gundogdu, J. H. Hou, H. Ade, *J. Mater. Chem. A* **2017**, *5*, 13176.

[90] C. Zhang, A. Mumyatov, S. Langner, J. D. Perea, T. Kassar, J. Min, L. Ke, H. Chen, K. L. Gerasimov, D. V. Anokhin, D. A. Ivanov, T. Ameri, A. Osvet, D. K. Susarova, T. Unruh, N. Li, P. Troshin, C. J. Brabec, *Adv. Energy Mater.* **2017**, *7*, 1601204.

[91] E. Gann, A. T. Young, B. A. Collins, H. Yan, J. Nasiatka, H. A. Padmore, H. Ade, A. Hexemer, C. Wang, *Rev. Sci. Instrum.* **2012**, *83*, 045110.

[92] C. Qian, S. J. Mumby, B. E. Eichinger, *Macromolecules* **1991**, *24*, 1655.

[93] P. Knychała, K. Timachova, M. Banaszak, N. P. Balsara, *Macromolecules* **2017**, *50*, 3051.

[94] R. A. Matkar, T. Kyu, *J. Phys. Chem. B* **2006**, *110*, 12728.

[95] P. Rathi, T.-M. Huang, P. Dayal, T. Kyu, *J. Phys. Chem. B* **2008**, *112*, 6460.

[96] H. Hu, K. Jiang, P. C. Y. Chow, L. Ye, G. Zhang, Z. Li, J. H. Carpenter, H. Ade, H. Yan, *Adv. Energy Mater.* **2017**, *7*, 1701674.

[97] T. Kurosawa, X. Gu, K. L. Gu, Y. Zhou, H. Yan, C. Wang, G.-J. N. Wang, M. F. Toney, Z. Bao, *Adv. Energy Mater.* **2017**, *7*, 1701552.

[98] P. P. Khlyabich, A. E. Rudenko, B. C. Thompson, Y.-L. Loo, *Adv. Funct. Mater.* **2015**, *25*, 5557.

[99] F. Gao, W. Tress, J. Wang, O. Inganäs, *Phys. Rev. Lett.* **2015**, *114*, 128701.

[100] K. Tvingstedt, C. Deibel, *Adv. Energy Mater.* **2016**, *6*, 1502230.

[101] J. D. A. Lin, O. V. Mikhnenko, T. S. van der Poll, G. C. Bazan, T.-Q. Nguyen, *Adv. Mater.* **2015**, *27*, 2528.

[102] C. B. Nielsen, S. Holliday, H.-Y. Chen, S. J. Cryer, I. McCulloch, *Acc. Chem. Res.* **2015**, *48*, 2803.

[103] Y. Lin, X. Zhan, *Mater. Horiz.* **2014**, *1*, 470.

[104] Y. Lin, J. Wang, Z.-G. Zhang, H. Bai, Y. Li, D. Zhu, X. Zhan, *Adv. Mater.* **2015**, *27*, 1170.

[105] Y. Lin, F. Zhao, Q. He, L. Huo, Y. Wu, T. C. Parker, W. Ma, Y. Sun, C. Wang, D. Zhu, A. J. Heeger, S. R. Marder, X. Zhan, *J. Am. Chem. Soc.* **2016**, *138*, 4955.

[106] Y. Lin, Q. He, F. Zhao, L. Huo, J. Mai, X. Lu, C.-J. Su, T. Li, J. Wang, J. Zhu, Y. Sun, C. Wang, X. Zhan, *J. Am. Chem. Soc.* **2016**, *138*, 2973.

[107] S. Dai, F. Zhao, Q. Zhang, T.-K. Lau, T. Li, K. Liu, Q. Ling, C. Wang, X. Lu, W. You, X. Zhan, *J. Am. Chem. Soc.* **2017**, *139*, 1336.

[108] F. Zhao, S. Dai, Y. Wu, Q. Zhang, J. Wang, L. Jiang, Q. Ling, Z. Wei, W. Ma, W. You, C. Wang, X. Zhan, *Adv. Mater.* **2017**, *29*, 1700144.

[109] P. Cheng, M. Zhang, T.-K. Lau, Y. Wu, B. Jia, J. Wang, C. Yan, M. Qin, X. Lu, X. Zhan, *Adv. Mater.* **2017**, *29*, 1605216.

[110] J. Wang, W. Wang, X. Wang, Y. Wu, Q. Zhang, C. Yan, W. Ma, W. You, X. Zhan, *Adv. Mater.* **2017**, *29*, 1702125.

[111] W. Wang, C. Yan, T.-K. Lau, J. Wang, K. Liu, Y. Fan, X. Lu, X. Zhan, *Adv. Mater.* **2017**, *29*, 1701308.

[112] Y. Lin, F. Zhao, Y. Wu, K. Chen, Y. Xia, G. Li, S. K. K. Prasad, J. Zhu, L. Huo, H. Bin, Z.-G. Zhang, X. Guo, M. Zhang, Y. Sun, F. Gao, Z. Wei, W. Ma, C. Wang, J. Hodgkiss, Z. Bo, O. Inganäs, Y. Li, X. Zhan, *Adv. Mater.* **2017**, *29*, 1604155.

[113] S. Li, L. Ye, W. Zhao, S. Zhang, S. Mukherjee, H. Ade, J. Hou, *Adv. Mater.* **2016**, *28*, 9423.

[114] L. Ye, Y. Xiong, Q. Zhang, S. Li, C. Wang, Z. Jiang, J. Hou, W. You, H. Ade, *Adv. Mater.* **2017**, *Revised*.

[115] L. Ye, W. Jiang, W. Zhao, S. Zhang, D. Qian, Z. Wang, J. Hou, *Small* **2014**, *10*, 4658.

[116] L. Ye, K. Sun, W. Jiang, S. Zhang, W. Zhao, H. Yao, Z. Wang, J. Hou, *ACS Appl. Mater. Interfaces* **2015**, *7*, 9274.

[117] D. Baran, R. S. Ashraf, D. A. Hanifi, M. Abdelsamie, N. Gasparini, J. A. Rohr, S. Holliday, A. Wadsworth, S. Lockett, M. Neophytou, C. J. Emmott, J. Nelson, C. J. Brabec, A. Amassian, A. Salleo, T. Kirchartz, J. R. Durrant, I. McCulloch, *Nat. Mater.* **2017**, *16*, 363.

[118] H. Bin, L. Gao, Z.-G. Zhang, Y. Yang, Y. Zhang, C. Zhang, S. Chen, L. Xue, C. Yang, M. Xiao, Y. Li, *Nat. Commun.* **2016**, *7*, 13651.

[119] J. Liu, S. Chen, D. Qian, B. Gautam, G. Yang, J. Zhao, J. Bergqvist, F. Zhang, W. Ma, H. Ade, O. Inganäs, K. Gundogdu, F. Gao, H. Yan, *Nat. Energy* **2016**, *1*, 16089.

[120] X. Y. Liu, L. Ye, W. C. Zhao, S. Q. Zhang, S. S. Li, G. M. Su, C. Wang, H. Ade, J. H. Hou, *Mater. Chem. Front.* **2017**, *1*, 2057.

[121] P. P. Khlyabich, A. E. Rudenko, R. A. Street, B. C. Thompson, *ACS Appl. Mater. Interfaces* **2014**, *6*, 9913.

[122] B. F. Hartmeier, M. A. Brady, N. D. Treat, M. J. Robb, T. E. Mates, A. Hexemer, C. Wang, C. J. Hawker, E. J. Kramer, M. L. Chabinyc, *J. Polym. Sci. Part B: Polym. Phys.* **2016**, *54*, 237.

[123] P. Cheng, X. Zhan, *Mater. Horiz.* **2015**, *2*, 462.

[124] P. Cheng, C. Yan, Y. Wu, J. Wang, M. Qin, Q. An, J. Cao, L. Huo, F. Zhang, L. Ding, Y. Sun, W. Ma, X. Zhan, *Adv. Mater.* **2016**, *28*, 8021.

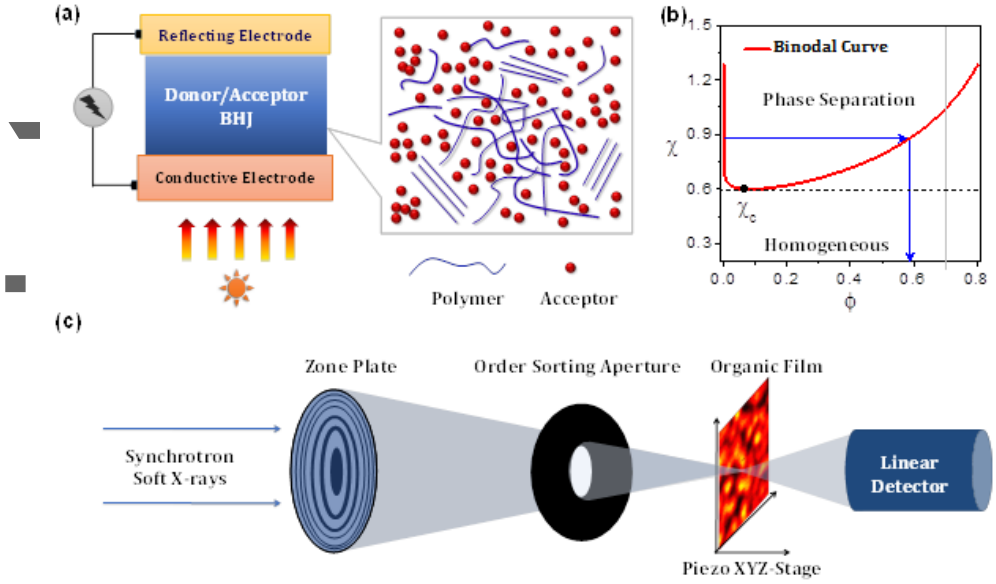

Figure 1. a) Schematic illustration of the three-phase morphology of a PSC blend whose existence requires a χ larger than the critical χ_c (see the black horizontal line shown in Figure 1b) and an aggregating/crystalline polymer. b) Simulated binodal, the coexistence curve in binary amorphous mixtures of a polymer:PCBM blend. Here φ is the composition of the donor polymer. The blue line indicates the composition of the mixed domain in the limit of complete phase separation at a given χ. In terms of miscibility, it is the amorphous miscibility that corresponds to the binodal. c) Schematic illustration of a transmission STXM previously developed at beamline 5.3.2.2, Advanced Light Source (ALS), Lawrence Berkeley National Laboratory. This STXM is a dedicated X-ray microscopy for polymer applications. Specifically, an incident soft X-ray beam can be focused onto a small spot and the order sorting aperture is used to filter the higher order diffracted light. An organic/polymer thin film is placed on a 3D sample stage and scanned in the focal plane of the zone plate and the transmitted soft X-ray intensity is recorded by the linear detector as a function of the sample position and energy. The reader is referred to the literature[34] for more details.

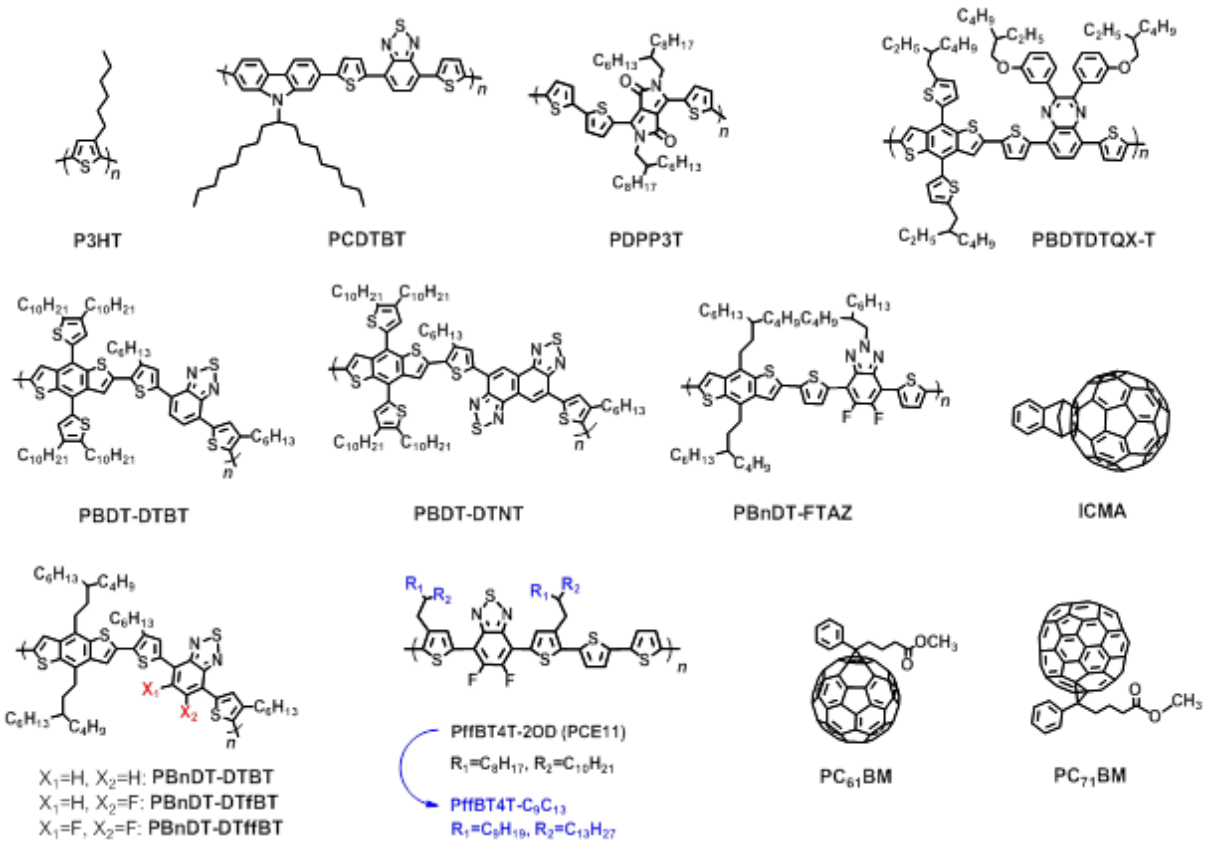

Figure 2. Chemical structures of donor polymers and acceptor materials used in the STXM liquidus miscibility measurements.

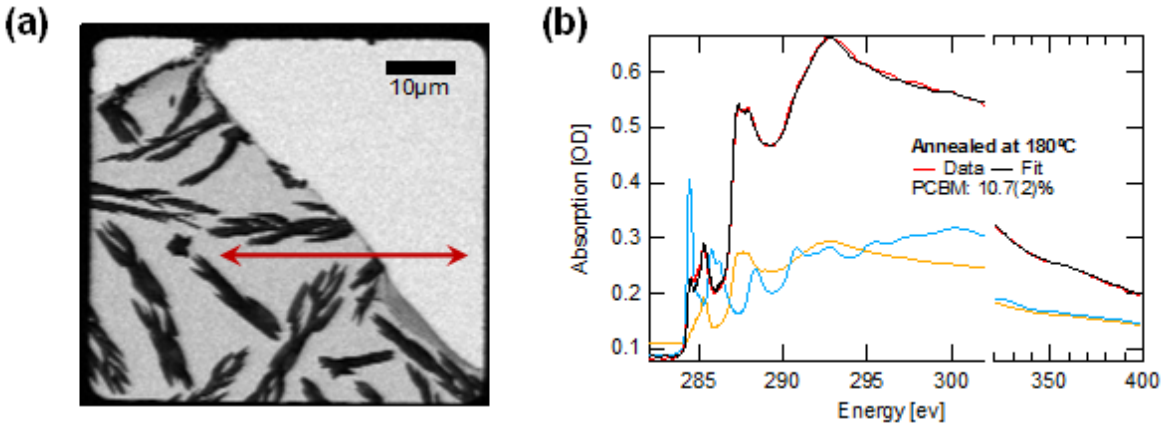

Figure 3. a) STXM image of an aggressively annealed regioregular P3HT:$PC_{61}BM$ blend film acquired at 284.4 eV, which corresponds to an absorption peak of $PC_{61}BM$. Dark regions are PCBM crystals. The arrow designates a typical line scan used to generate a spectrum. b) Fits of regioregular P3HT:$PC_{61}BM$ blend film spectra after annealing at 180 ^{o}C for 2 days. Yellow and blue curves are reference spectra of neat P3HT and $PC_{61}BM$ films, respectively. Reproduced with permission.[17] Copyright 2010, American Chemical Society.

Table 1. The measured liquidus miscibility data and the device parameters of various PSC blend systems.

D:A Systems	V_{oc} [V]	J_{sc} [mA cm^{-2}]	*FF* [%]	*PCE* [%]	Uncorrected Liquidus Miscibility[a] (Temperature)	Ref.
PffBT4T-2OD:ICMA	0.78	16.4	77	9.8	3.2% (130 °C)	[32]
PDPP3T:$PC_{71}BM$	0.66	15.0	66	6.51	4.5% (180 °C)	[46]
PBnDT-DTBT:$PC_{71}BM$	0.78	11.7	47.6	4.33	21% (20 °C)[b]	[37]
PBnDT-DTfBT:$PC_{71}BM$	0.84	11.5	52.2	4.91	16% (20 °C)[b]	[37]
PBnDT-DTffBT:$PC_{71}BM$	0.90	12.2	62.1	6.64	12% (20 °C)[b]	[37]
PBDT-DTBT:$PC_{71}BM$	0.93	5.08	29	1.37	35.6% (190 °C)	[28]
PBDT-DTNT:$PC_{71}BM$	0.79	13.23	59	6.14	5.0% (190 °C)	[28]
PBDTDTQx-T:$PC_{71}BM$	0.76	11.35	60	5.17	11% (180 °C)	[47]
PBnDT-FTAZ:$PC_{61}BM$	0.77	13.1	69	7.0	3.7% (20 °C)[b]	[40]

a) Residual fullerene weight fraction in the polymer matrix.

b) Solvent annealed using trichlorobenzene.

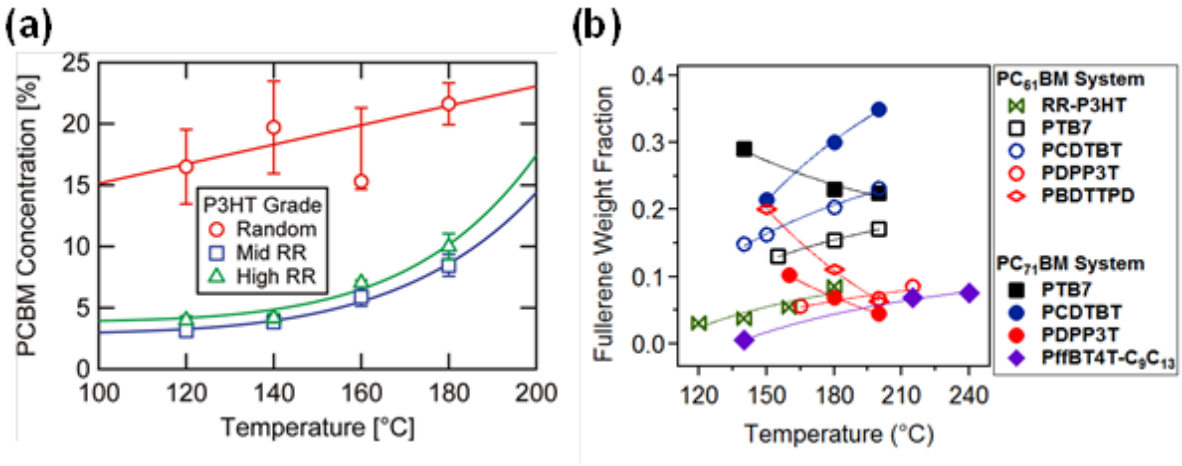

Figure 4. a) Temperature-dependent liquidus miscibility for P3HT mixed with $PC_{61}BM$. Lines are guides for the eye. Reproduced with permission.[17] Copyright 2010, American Chemical Society. b) Residual fullerene ($PC_{61}BM$ or $PC_{71}BM$) weight fractions in a number of representative donor polymers as a function of temperature. Lines are fits to y=A+B/x (A and B are constants) after taking into account a constant DoC. It is clear that RR-P3HT:PCBM system would need an additional C/x^2 term to get a better fit.

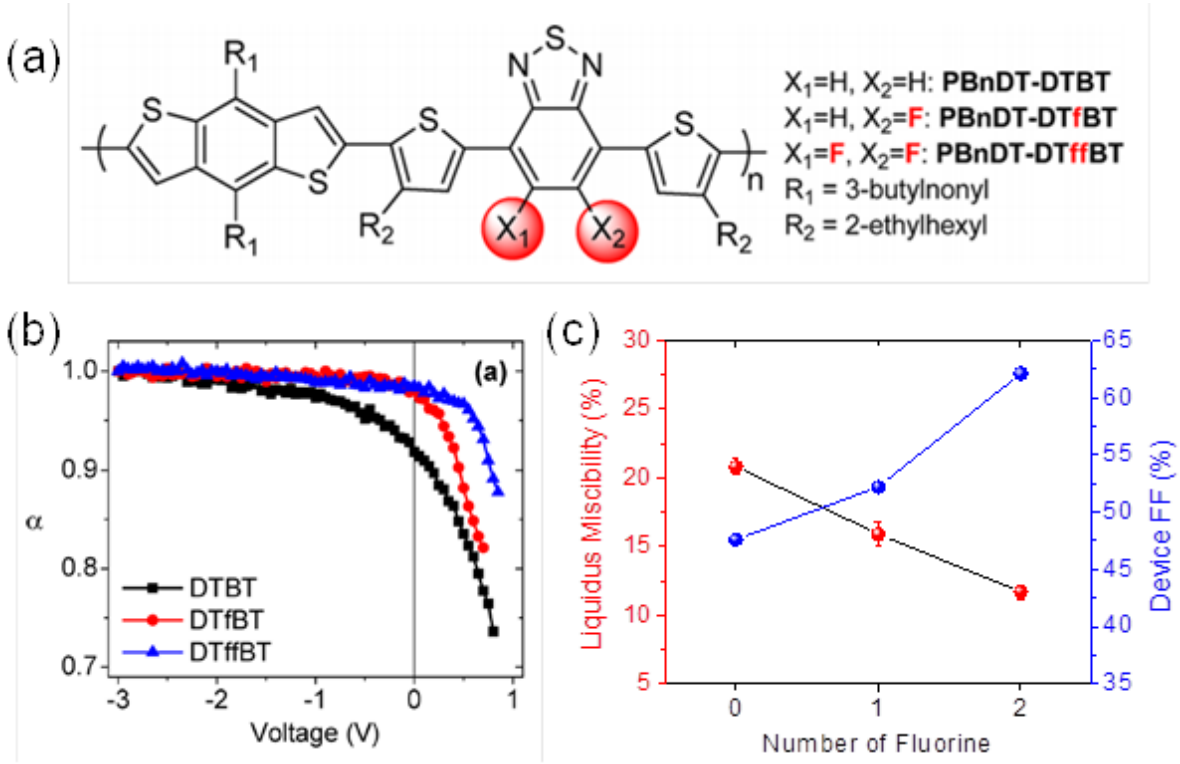

Figure 5. a) Chemical structures of three donor polymers: PBnDT-DTBT ("0F"), -DTfBT ("1F") and -DTffBT ("2F"). b) Plot of scaling exponent as a function of voltage for 0F, 1F, and 2F-based PSC devices with 200 nm film thickness. c) Liquidus miscibility (residual fullerene concentration) and device FF as a function of fluorine number in the donor polymer. Reproduced with permission.[37] Copyright 2013, American Chemical Society.

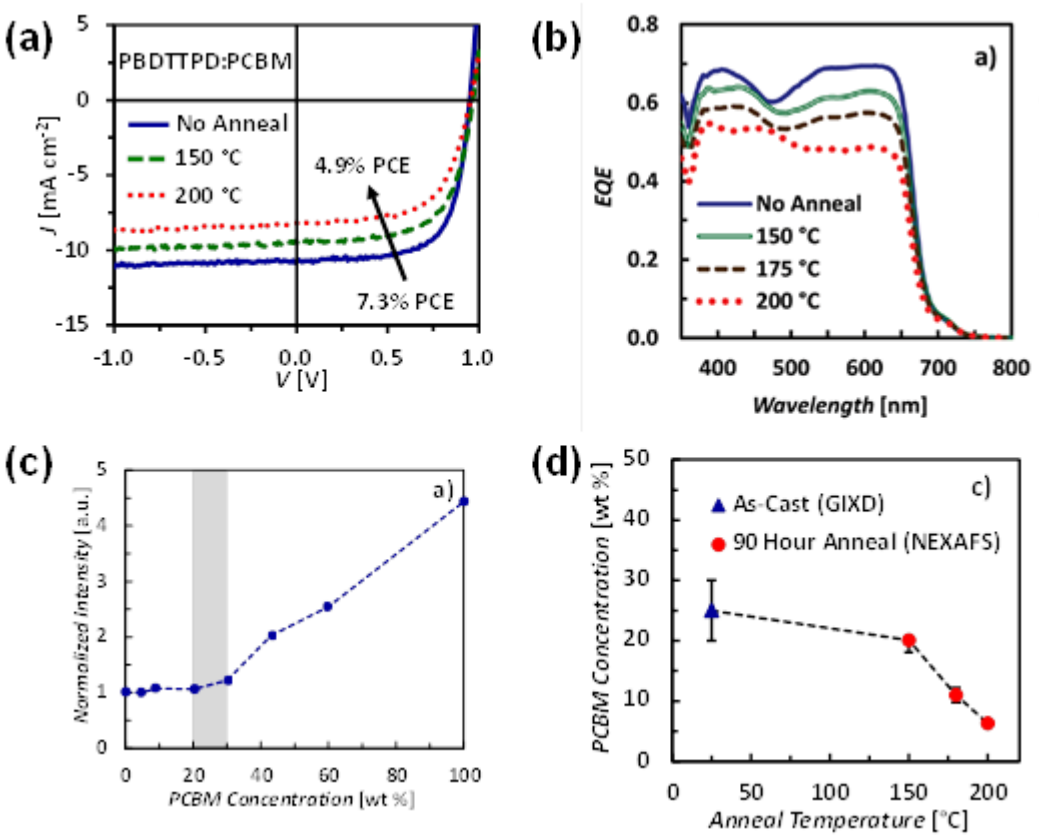

Figure 6. a) *J-V* curves of PBDTTPD:$PC_{61}BM$ devices annealed at different temperatures. b) External quantum efficiency curves of as-cast and thermally annealed PBDTTPD:$PC_{61}BM$ solar cells. c) Normalized grazing incidence X-ray diffraction intensity ($PC_{61}BM$ peak q= 0.7 $Å^{-1}$) as a function of the PCBM concentration in the PBDBTPD:$PC_{61}BM$ BHJs. The grey band marks the estimated concentration of as-cast $PC_{61}BM$ mixed in PBDTTPD. d) Residual weight ratio of $PC_{61}BM$ in PBDTTPD as a function of temperature. Reproduced with permission.[39] Copyright 2013, Wiley-VCH.

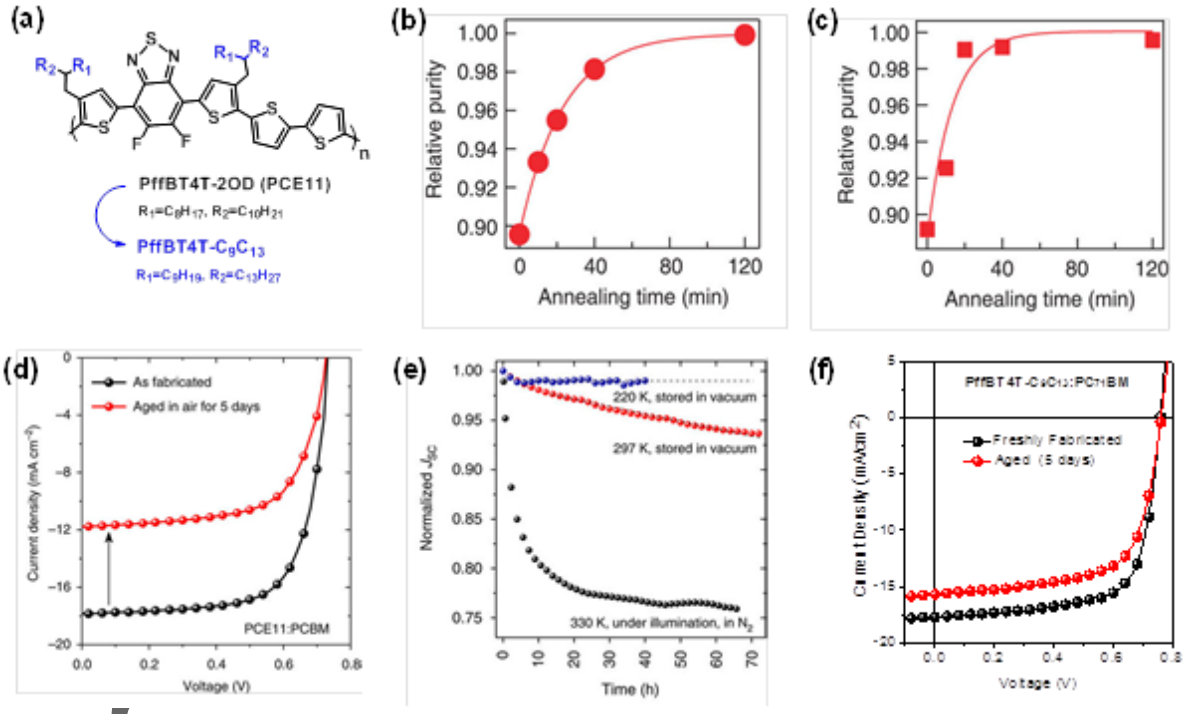

Figure 7. a) Chemical modifications of PffBT4T polymers. Relative phase purity as a function of annealing time for b) PffBT4T-2OD:ICMA and c) PffBT4T-2OD:$PC_{71}BM$. Reproduced with permission.[32] Copyright 2017, Nature Publishing Group. d) *J-V* characteristics of optimized PffBT4T-2OD:$PC_{61}BM$ PSCs measured after fresh fabrication and after aged in air for 5 days (aged). e) Evolution of J_{sc} of optimized PffBT4T-2OD:$PC_{61}BM$ solar cells measured at different temperatures in vacuum. Reproduced with permission.[62] Copyright 2017, Nature Publishing Group. f) Representative *J-V* characteristics of PffBT4T-C_9C_{13}:$PC_{71}BM$ devices measured after freshly fabricated and aged for five days (in an inert atmosphere).

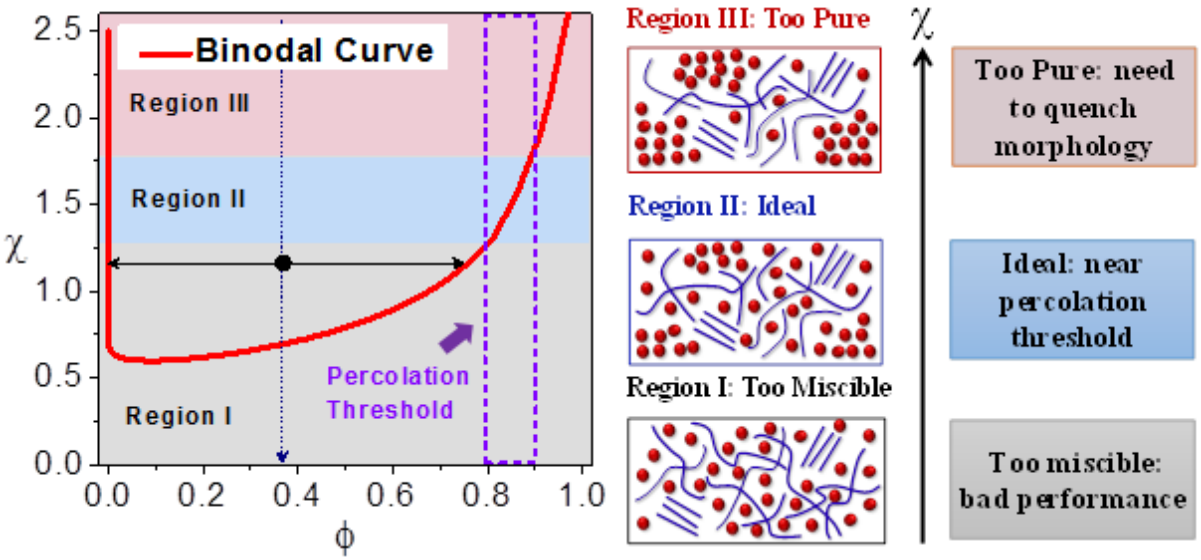

Figure 8. Schematic illustration of three regimes in the χ-φ phase diagram. Regime I, II, III represent high χ, medium χ (where purity of mixed domain is close to the fullerene percolation threshold), and low χ, respectively. The dashed rectangle marks the reported percolation threshold values[39, 65] where polymer volume fractions are 0.8-0.9.

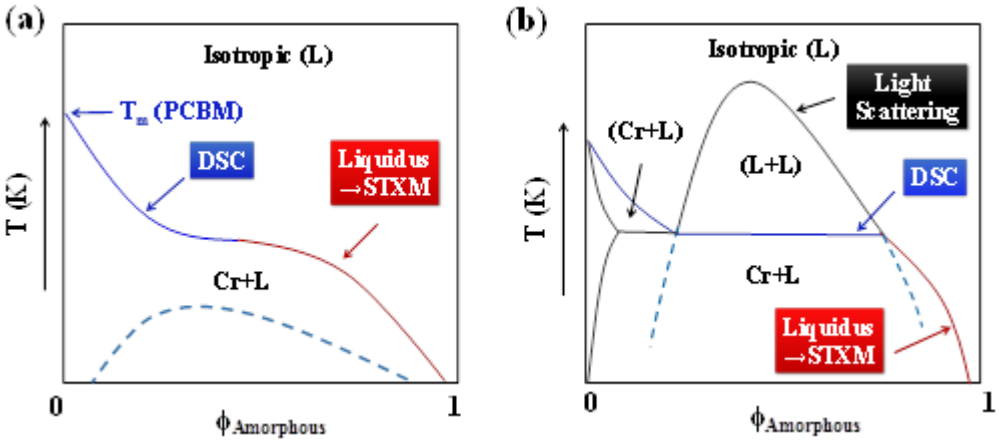

Figure 9. Nominal crystalline-amorphous phase diagram for a) a high miscibility (low χ) system and b) a low miscibility (high χ) UCST system. The proposed methods to measure the most important transitions of polymer:PCBM systems are as indicated. Metastable miscibility gap is indicated as dashed lines. The diagram, particularly the binodal (L-L boundary) will be asymmetric if there is a difference in the molecular weight of the two components. T_m is the melting point of neat PCBM. Schematic modeled after P. Rathi et al. [95]

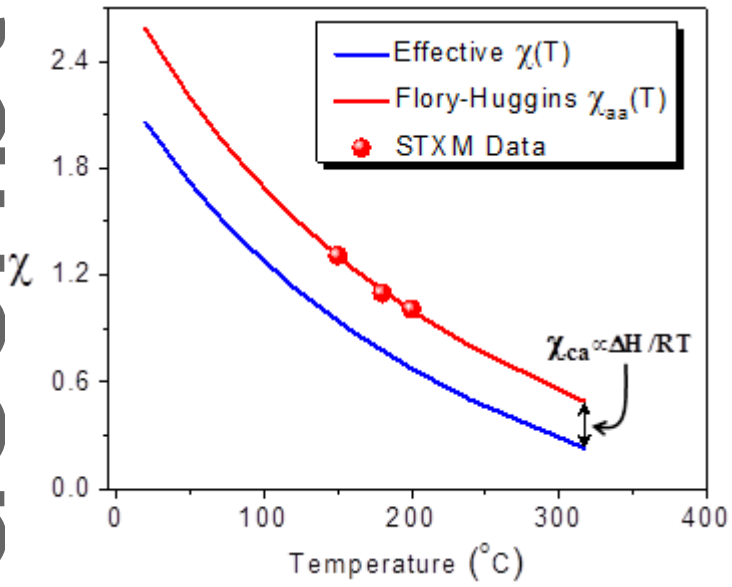

Figure 10. Effective χ estimated from STXM (red dots) as a function of T, and derived $\chi_{aa}(T)$ of PCDTBT:$PC_{71}BM$ blend. Red line is a fit to $\chi(T)=A+B/T$, where A and B are constants. The difference between effective χ and χ_{aa} is calibrated by $\chi_{ca}(T_m)$ estimated by DSC melting point depression.[68]

Author Biographies

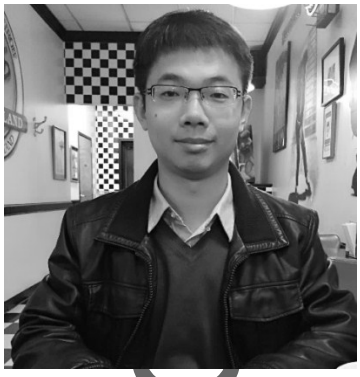

Long Ye is a postdoctoral research associate working with Prof. Harald Ade at the Department of Physics, North Carolina State University (NCSU). He received his Ph.D. in July 2015 at the Institute of Chemistry, Chinese Academy of Sciences (ICCAS). His research focuses on developing high-efficiency eco-friendly organic solar cells by scalable methods, and characterizing, manipulating, and predicting the complex morphology of organic/polymeric semi-conducting blends in photovoltaic devices.

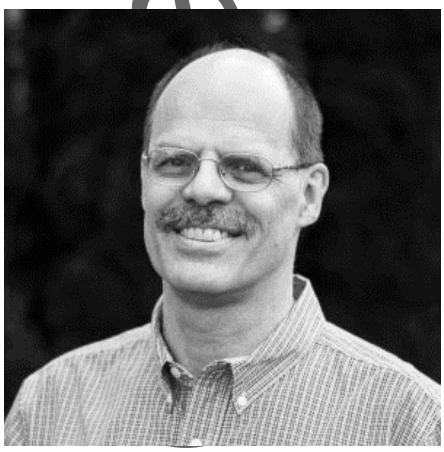

Harald Ade is a Goodnight Innovation Distinguished Professor and Director of Organic and Carbon Electronics Laboratory (ORaCEL) at NCSU. He received his Ph.D. in physics from SUNY at Stony Brook (now Stony Brook University) in 1990 and has been a faculty member at NCSU since 1992. He is developing and using novel soft X-ray characterization tools (microscopy, scattering, reflectivity, etc), with a focus on the characterization of organic devices.

The significance of miscibility and its temperature dependence in controlling morphology, performance, and stability of polymer:fullerene solar cells is discussed. Highly variable miscibility is observed for a wide range of systems and can be converted to temperature-dependent effective Flory-Huggins interaction parameter (χ). There is an optimum miscibility near the fullerene percolation threshold for most efficient and stable solar cells.

Keyword: polymer solar cells

L. Ye, B. A. Collins, X. C. Jiao, J. Zhao, H. Yan, and H. Ade*

Miscibility-Function Relations in Organic Solar Cells: Significance of Optimal Miscibility in Relation to Percolation

ToC figure